Analysis of 37 kW Converter-Fed Induction Motor Losses

Lassi Aarniovuori, *Member, IEEE*, Paavo Rasilo, Markku Niemelä, and Juha Pyrhönen, *Member, IEEE*

Abstract—This paper presents an energy efficiency analysis of a 37 kW standard squirrel-cage induction motor under sinusoidal and non-sinusoidal supply. The motor losses are analyzed using the conventional IEC loss segregation method and also numerically modeled using finite element simulations. The measured and simulated loss components are compared with three different modulation methods. The overall simulated losses are in good agreement with the measured ones, but there exist differences in the loss components.

Index Terms— AC motors, induction motors, magnetic losses, numerical simulation, power semiconductor switches pulse-width modulation converters, variable-speed drives (VSDs)

I. INTRODUCTION

VOLTAGE source converter is the most common type of converter in the industrial motor applications. The two-level voltage-source converters have been used since the 1970's to supply induction motors in variable speed applications. In the near future induction motor drives equipped with pulse-width-modulated (PWM) converters will also have their own efficiency classification as well as an internationally accepted measurement method to determine the losses [1]. There are two different measurement methods suitable for determining the total losses of all electrical motor types; the input-output method and the calorimetric method. In the first one the losses of the motor are simply the difference of the electrical input power and the mechanical output power. Because of the measurement device properties the input-output method becomes relatively inaccurate when the efficiency is approaching unity or the electrical waveforms are heavily distorted. The calorimetric method is slow, complex and troublesome to arrange and it can, therefore be used only in special cases [2],[3]. The problem of the aforementioned methods is that they can only be used to obtain the total losses

L. Aarniovuori, M. Niemelä, and J. Pyrhönen are with the Department of Electrical Engineering, Lappeenranta University of Technology (LUT), Lappeenranta, Finland (e-mail: lassi.aarniovuori@lut.fi; markku.niemela@lut.fi; juha.pyrhonen@lut.fi).

P. Rasilo is with the Department of Electrical Engineering, Tampere University of Technology, Tampere, Finland and with the Department of Electrical Engineering and Automation, Aalto University, Espoo, Finland (e-mail: paavo.rasilo@tut.fi).

TABLE I
TEFC MOTOR PARAMETERS FOR DELTA CONNECTION

Variable	Value
Power, P_N (kW)	37
Current, I_N (A)	65.4
Voltage, U_N (V)	400
Torque, T_N (Nm)	239
Frequency, f_N (Hz)	50
Speed, n_N (rpm)	1482
Efficiency, η (%)	94.9 (IE3)

of the machine. The result includes both the electromagnetic and the mechanical losses. The most commonly used method to segregate the losses is given in IEC standard [4] and a similar procedure is used also in IEC Technical Specification [5] to extract the harmonic losses from the total losses. Another way to analyse the loss components and to increase the knowledge on where the losses take place is to use analytical equations or finite element (FE) analysis. The FE analysis is more time consuming but more precise and includes the effects of the machine geometry, but naturally it cannot include all the non-idealities of the real machine.

In this paper, we compare the loss segregation procedures IEC 60034-2-1 Edition 2 of [4] and IEC 60034-2-3 TS [5] to detailed FE analysis of the different loss components. The aim is to numerically check the validity of the standardized loss segregation methods. A 37 kW four-pole, 400 V, 50 Hz induction motor is used as the test machine. The name plate values of the motor are given in Table I. For the simulations, a 2D FE model is used that was created using detailed information provided by the motor manufacturer. The FE model is coupled to a dynamic iron-loss model which accounts for the hysteresis, eddy-current and excess losses in the core laminations. To include the time harmonics created by the PWM-supply to the FE-analysis, voltage waveforms recorded from the machine terminals are used to supply the model. Another but more exhausting method would be to model also the converter and its control system and couple it to the FE-software [6]. The new European Standard [7],[8] gives reference motor losses which are equal to IE2-class motors added with 25 % of harmonics losses created by PWM-supply. We are still waiting for the official standard IEC 60034-2-3 [9] and there still exists arguing about what should be the correct operational point for a PWM-fed machine type testing. Here, 400 V converter input voltage is used. It equals the motor nominal voltage and it is the most used voltage level in European industrial applications and gives the most realistic loss results in the case of converter fed induction motors. A problem, however, is related to this voltage supply; because of

the voltage drop and the modulation principles the motor will operate in field weakening at its rated 50 Hz frequency in converter supply.

II. STANDARD LOSS SEGREGATION

According to [4] induction motor losses can be divided in five parts; stator copper losses, rotor copper losses, iron losses, mechanical losses and additional load losses. These loss components can be denoted as "conventional" or "standardized" loss components and the additional load losses includes all other losses that cannot be modelled using the analytical equations. These conventional loss components cannot be considered as an absolute truth, but the calculation procedure is well known, generally accepted and understood in the community of electrical machine experts. In the following, all the quantities are assumed to represent steady-state values at the end of the heat-run rest, if not mentioned otherwise.

A. Stator copper losses

The stator copper losses are calculated according to the IEC norm by using the test resistance R_H and current I_H values

$$P_s = 1.5 R_H I_H^2 = 3 R_{pH} I_H^2, \qquad (1)$$

where I_H is the stator phase current and R_H is the winding line-to-line resistance. Naturally this gives the same result as the latter part with the phase resistance R_{ph}. There are a few different ways to determine the test resistance, but according to IEC it is the DC-resistance of the stator winding at the temperature equal to thermal equilibrium reached at the end of the heat run test. This indicates that according to IEC norm skin- and proximity-effect-caused losses are included in the additional load losses. In the case of a PWM-fed machine a better approximation could be achieved by using AC-resistance instead.

B. Rotor copper losses

The rotor winding losses are slip (s) related and are typically calculated with the well know equation

$$P_r = (P_1 - P_s - P_{Fe})s, \qquad (2)$$

where P_1 is the electric input power, P_s is the stator winding losses, P_{Fe} is the iron loss from the no-load test and s is the slip. This equation has an inherent mistake in itself as it ignores the additional losses, which naturally are included in P_1. The mistake is, however, negligible as the slip s as the multiplicator of the small error is also small.

C. Iron losses and mechanical losses

The constant losses are defined by subtracting the stator resistive losses $P_{s,0}$ from the electric input power P_0 during the no-load test

$$P_c = P_0 - P_{s,0} = P_{fw} + P_{Fe} \qquad (3)$$

that is equal to the friction and windage losses P_{fw} and iron losses P_{Fe}. The friction and windage losses are calculated from

four or more constant loss points between approximately 60 % and 30 % of voltage by developing a curve against no load voltage squared (U_0^2) and extrapolating to a zero voltage. The iron losses are calculated using the no-load test voltage points from 90% to 110% of rated voltage. A curve of

$$P_{Fe} = P_c - P_{fw} \qquad (4)$$

against no load voltage (U_0) is created. The iron losses are determined in the inner voltage point U_i that takes the resistive voltage drop in the primary winding into account and is calculated as

$$U_i = \sqrt{(U - I_{ph}R_{ph} \cos \varphi)^2 + (I_{ph}R_{ph} \sin \varphi)^2}. \qquad (5)$$

Naturally, (5) is, in theory, valid for sinusoidal supply and ignores the frequency effects on the phase resistance. In a typical case the stator resistance per-unit value is in the range of 0.02. If the resistance factor is small the mistake made here in the inner voltage is also negligible, typically less than 1 %.

One of the problems in the comparison of the calculated and measured losses is how to determine the mechanical losses accurately [10]. The mechanical losses are dependent on complicated aerodynamic friction phenomena [11] which depend on the rotational speed. Also the amount of lubrication grease in the bearings has an impact. Friction losses tend to vary as a function of time. Mechanical losses are temperature dependent as has been shown e.g. in [12]. The mechanical losses are removed from the measured losses and we can assume that they remain constant because the temperature and rotational speed of all analyzed points are relatively close to each other. Here, the value of 152 W is used for friction and windage losses and can be considered a as a "hot machine" value [12]. The loss has been calculated based on the retardation test.

D. The additional load losses

The additional load losses are often referred as "not clearly known" losses that include e.g. the extra losses caused by the current linkage harmonics created by stator windings, permeance harmonics produced by stator and rotor slots, saturation harmonics from core laminations and the extra losses caused by the difference of AC and DC resistance. In the IEC standard the additional load losses are evaluated calculating the residual loss (P_{Lr}) at each load point of the load curve test.

$$P_{Lr} = P_1 - P_2 - P_s - P_r - P_{Fe} - P_{fw}, \qquad (6)$$

where P_2 is the mechanical shaft power. The residual losses are expected to be a function of torque squared and the additional loss value is obtained using the linear regression analysis. There are a few different methods to determine the stray losses experimentally, but the results obtained with different methods are not in good agreement [13].

III. MODULATION METHODS

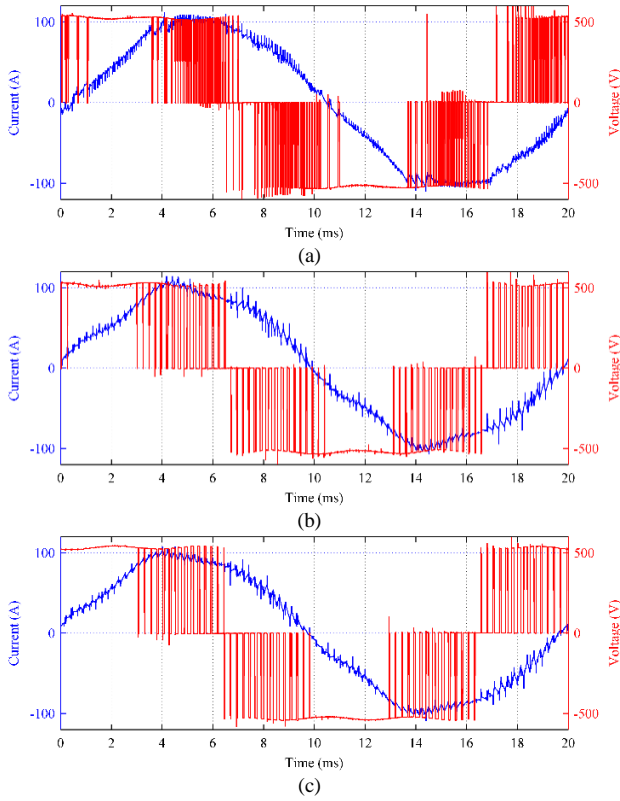Different converter power-stage switches' modulating methods produce different kinds of voltage waveforms and

Fig. 1. One fundamental wave period of the measured current (left axis) and line-to-line voltage (right axis) waveforms as a function of time in the motor nominal load point (a) Direct torque control (b) Space vector modulation. (c) Symmetrical two-phase modulation.

spectra to the motor terminals. Various different modulation methods have been proposed in the literature and good explanations of the modulation methods can be found e.g. in [14] and [15]. Here, three commercial converters that utilize the three different modulation methods were used. The three-phase voltage waveforms were captured and true IGBT switching instants were extracted from the data to compare the motor losses against the true switching frequency. Here we have to distinguish between the terms carrier frequency and switching frequency. The switching frequency is the number of the switching instants at some time interval and the carrier frequency is the fixed frequency that defines the potential switching instants. In the carrier based modulation the carrier frequency is therefore the maximum switching frequency and true switching frequency is often smaller than that. The modulation or control methods are denoted here as 1: direct torque control (DTC), 2: space vector modulation (SVM) and 3: symmetrical two-phase modulation (DPWM). The methods are introduced here only briefly. The measured voltage and current waveforms are shown in Fig. 1 in the time domain and in the Fig. 2 in the frequency domain from the motor nominal load point. Since the focus in this paper is not on the modulation methods, the converter is denoted here only as a voltage supply for motor. It can be examined from Fig. 1 that the SVM and DPWM modulators creates very similar waveforms in this operating point. The motor terminal voltage is also shown in the stator coordinates to show the modulation depth and modulating waveform, Fig. 2. The measured stator voltage is filtered only for illustrative purposes with a 4th order

low-pass filter with a cut off frequency of 500 Hz to reveal the modulation waveform. The 500 Hz cut off frequency may not be optimal, but that is used also in [5] and when the same filtering frequency is used for all methods, it is valid for comparison. The filtered voltage waveform in stator coordinates can be used to compare the state of the machine with different voltage supplies. When observing the total losses of the machine in Fig. 4, it can be seen that a higher fundamental voltage leads to lower losses and the role of the voltage harmonics is actually minor. It can be easily seen in Fig. 2 that the DTC converter produces the lowest amplitudes for low level (up to 10) harmonics in this case. The data in the frequency domain is calculated using DFT with a rectangular window that is synchronized with the fundamental frequency [16].

A. Direct Torque Control (DTC)

Direct torque control (DTC) is one type of PWM control strategy which can be considered as an alternative for vector control technique. DTC was proposed for AC drives by Depenbrock and Takahashi in the 1980s [18], [19]. It has the advantages of fast torque response, simple design and robustness against motor parameter variations. The variable switching frequency and high torque ripple may be in some cases regarded as drawbacks of the classical DTC. Direct torque control has been a topic of numerous scientific works over the past two decades; the switching frequency of the DTC is analysed in [20] and [21]. Numerous improvements in the classical DTC have been proposed for instance in [18]-[27]. From the harmonic loss analysis point of view, the DTC is a really interesting control method, since it does not have a constant switching frequency similar to the more commonly used carrier based methods, such as the SVM. Also, the fixed time step realization used here with 25 µs time steps gives the upper limit of 40 kHz to the frequency band of the electric power that has to be observed. The main principle of the DTC is to control the torque and the modulus of the stator flux linkage directly by controlling the inverter switches using the outputs of the hystereses comparators and selecting the correct voltage vector from the optimal switching table [28]. The estimate of the stator flux linkage vector $\Psi_{s,est}$ is calculated with the integral

$$\Psi_{s,est} = \int (u_s - r_s i_s) dt, \qquad (7)$$

where u_s is the voltage and i_s is the measured current vector. The calculation is performed in a two-axis reference frame fixed to the stator coordinates. The estimate of the electromagnetic torque is calculated from the estimated flux linkage components and the measured stator currents in the reference frame as

$$T_{e,est} = \frac{3}{2} p (\psi_{s\alpha} i_{s\beta} - \psi_{s\beta} i_{s\alpha}) \qquad (8)$$

In the DTC there is no fixed switching frequency but the average switching frequency is controlled with flux linkage and torque hysteresis bands. The hysteresis bands are controlled by the reference switching frequency to achieve the desired average value. In the DTC, there is no predetermined switching pattern either, and the harmonic contents of the voltages is not known beforehand. The difference between

standard PWM methods and the DTC lies in the switching mode; in the classical PWM, the switching follows a sequential pattern, while in the DTC method, the switching is controlled by torque and flux linkage errors. As a result, the DTC method should ensure simultaneous minimization of both the pulsation and switching frequency. The above features are necessary to improve not only the technical properties of the drive (i.e. decrease of speed pulsation) but also its economic characteristics, as the switching frequency influences the power losses, and hence, the inverter efficiency.

B. Space Vector Pulse Width Modulation

The space vector modulation (SVM) is one of the modulation techniques that are used together with vector control. SVM can be considered as a standard for switching power converters [29]. In the space vector PWM the output voltage vector $\boldsymbol{u(t)}$ can be written as

$$\boldsymbol{u(t)} = \frac{t_0}{T_s}\boldsymbol{u}_0 + \frac{t_a}{T_s}\boldsymbol{u}_a + \frac{t_b}{T_s}\boldsymbol{u}_b + \frac{t_7}{T_s}\boldsymbol{u}_7, \quad (9)$$

where the t are the turn-on times of the vectors, T_s is the sampling time and subscripts 0 and 7 refer to zero vectors and a and b in the two adjacent voltage vectors in an arbitrary sector. Diverse SVPWM-schemes can be produced by distributing the zero vectors with certain ways. Here, the most common modulation is used where the zero vectors $\boldsymbol{u}_0$ and $\boldsymbol{u}_7$ are both used in one switching sequence and distributed evenly [30]. The zero vector is chosen based on the least number of switchings to produce the corresponding zero vector.

C. Symmetrical Two-Phase Modulation

The vector control is also utilized with the symmetrical two phase modulation. That is one of the discontinuous modulation methods (DPWM). Some references denote the modulation method as DPWM1 method. In symmetrical two-phase modulation to avoid unnecessary switchings and to improve the converter efficiency, one of the three phases is clamped by 60 degrees either to the lower or upper DC bus, and only two phases are switched. In theory, the two-phase modulation provides a 33 % reduction in the effective switching frequency and switching losses compared with the standard SV-PWM. The modulation method has a high current harmonic content at a low modulation index.

IV. MEASUREMENTS

The experimental tests were performed using the state-of-the-art equipment and a computer aided data acquisition with truly digital communication. The measurement data is directly read from the measurement instrument in digital format without any additional conversions. The electrical input power was measured with Yokogawa PZ4000 power analyzer which was equipped with a 500 kHz bandwidth Zero-Flux current measurement system and the mechanical power was gathered with HBM T12 torque transducer using CAN-bus. The total measured losses with the three different modulation methods are presented in Fig. 4 together with sinusoidal supply losses. It can be examined that the absolute wattage difference is increasing between the sinusoidal and PWM-supply when the
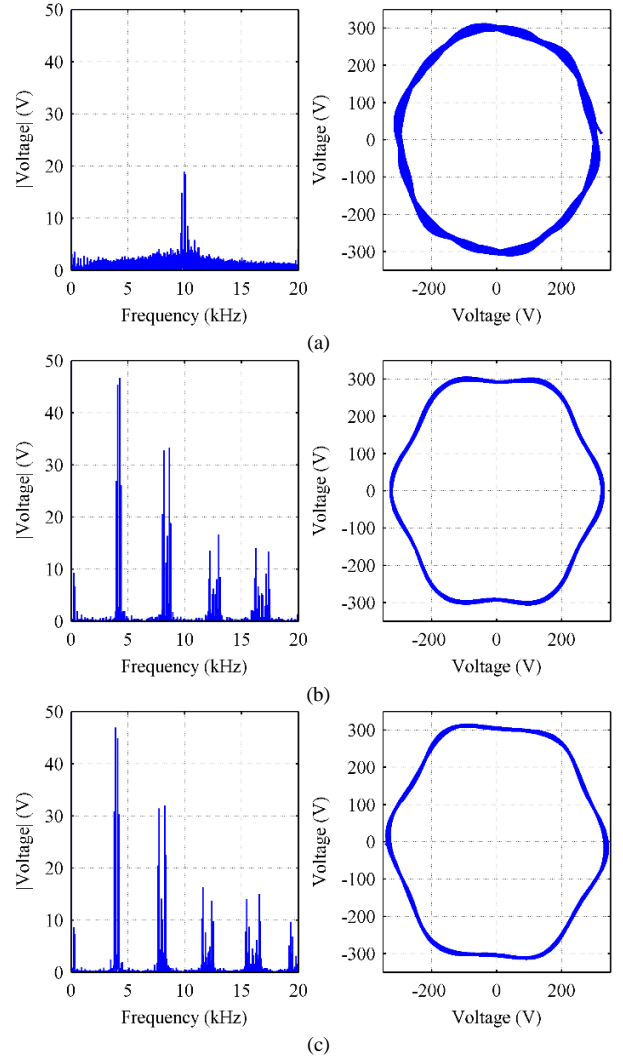

Fig. 2. The measured voltage waveforms presented in frequency domain (left) and in the stator coordinates (right). (a) Direct torque control. The fundamental RMS phase-voltage value is 212.1 V. The round locus shows that DTC keeps the voltage fairly sinusoidal. The spectrum is spread over a wide frequency band that is typical for stochastic DTC-modulation. (b) Space vector modulation. The fundamental phase voltage RMS value is 219.4 V. The carrier frequency and side bands are seen from the spectrum. (c) Symmetrical two-phase modulation. The fundamental phase voltage RMS is 225.3 V. The carrier frequency and its side bands are seen in the spectrum. Both latter modulation methods go in overmodulation resulting in more or less hexagonal voltage loci.

load is increased. The motor losses are very close to each other with all three modulation methods. The truly utilized switching frequencies are gathered in Table II. In Fig. 3 the THD$_{50}$ that includes the first 50 harmonics values of the voltage and current are given. The THD values of the measured voltage and current waveforms in the different load points in Fig 3. are calculated according to "IEEE Standard 519 – IEEE Recommended Practice and Requirements of Harmonic Control in Electric Power Systems" [31] and are scaled with a fundamental wave amplitude. It can be examined from Fig. 3 that the voltage THD values of the both carrier based modulation methods are very close to each other and the THD of the DTC voltage is much higher than the ones with

TABLE II
THE TRUE SWITCHING FREQUENCIES (HZ) OF THE ANALYZED WAVEFORMS.

Load	DTC	PWM	DPWM
115%	2985	1735	1554
100%	2980	1744	1582
75%	3005	1675	1524
50%	2986	1644	1540
25%	2993	1600	1494
0%	2999	1998	2007

carrier based modulation. The current THD values are at the maximum with 25 % of the load and they are decreasing as the load is increased.

It is easily seen in Table II results that even when in the carrier based modulation carrier frequency is 4 kHz, in reality the number of switching instants are far away from 4 kHz, near 2 kHz or lower. The theoretical value for PWM is 4 kHz and DPWM 2.66 kHz but when there is not enough voltage to be utilized, the short periods in the switching pattern are not realized. Therefore, there are switching patterns that include only one active vector instead of two active vectors and zero vector. Overmodulation is the main explanation for the low switching frequency compared to the carrier frequency. It can be seen from Fig. 1. that there are long periods without any switching instants. On the other hand, in DTC the average switching frequency is controlled with the torque and flux hysteresis bands and therefore it is almost constant with all loads. The consequence of switching frequency can be also seen from the right column Fig. 2. with DTC and with remarkable higher true switching frequency the modulating waveform looks more circular than with the carrier-based modulation and lower switching frequency. When examining the voltage spectra in the Fig. 2 and the overall losses in Fig. 4, it can be concluded that when the motor is fed with very different waveforms, but still the losses can be very close to each other.

V. NUMERICAL SIMULATIONS

The motor is simulated with a 2-D FE model based on a magnetic vector potential formulation. The FE mesh with 2nd order triangular elements is shown in Fig. 5 (a). The field equations are coupled to circuit equations of the stator windings. The rotor cage is modelled by choosing the bar potential differences as the state variables and writing circuit equations for the bars and the end-rings (p. 40-44 of [32]). Analytical methods have been used to estimate the stator end-winding inductance as well as the inductance and resistance of the rotor end ring (p. 80-81 of [33]). The stator winding is supplied with the measured voltage waveforms, and the stator current and current density of the rotor bars are solved together with the field. The stator copper losses are calculated from the phase currents using the measured stator winding resistance and temperature. Otherwise, the FEM model is not tuned, but the same calculation parameters are used for all modulation methods. However, individual stator winding strands are not modelled and thus possible conductor skin effect or losses caused by circulating currents are not included in the solution. In a winding manufactured of round enamelled wires with small diameter this is not a large source of error.
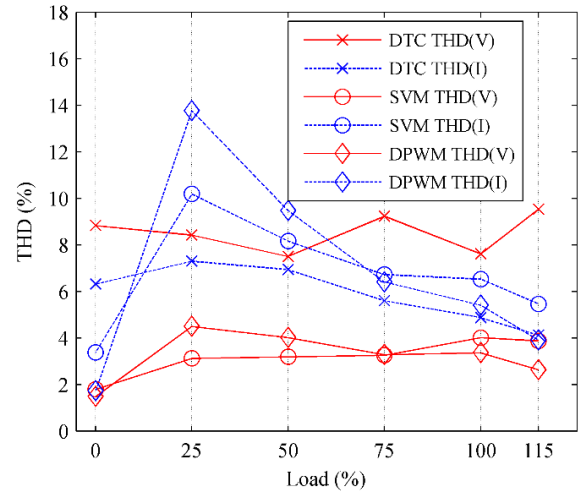

Fig. 3. THD values of the measured voltage and current with different PWM supplies as a function of motor load.
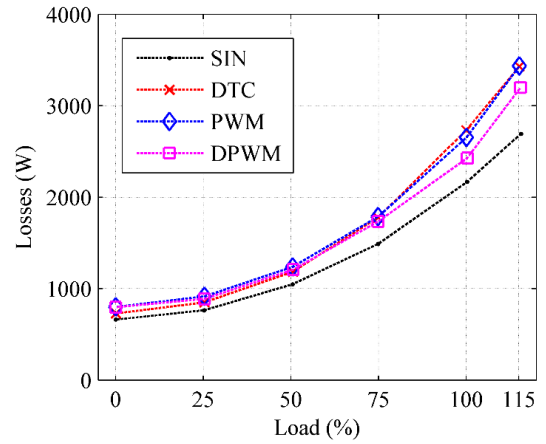

Fig. 4. Overall measured losses of the 37 kW induction machine with different modulation methods compared to sinusoidal supply. The overall losses includes the friction and windage losses.

The iron losses are included in the FE solution using the method described in [34]. The loss model is based on solving the flux-density distribution in the thickness of the core laminations taking into account the skin effect of the eddy currents. The model is able to describe the arbitrary time-variation and rotation of the flux-density vectors in the core. A single valued *BH*-curve is used during the simulation, and the hysteresis and excess losses are calculated in the post processing using a vector Preisach model and a dynamic excess-loss model. The magnetization curves used for the core material are given in Fig. 5 (b).

VI. RESULTS AND DISCUSSION

A. Total Losses

The measured and simulated total electromagnetic losses are compared in Fig. 6. With DTC supply, the simulated and measured total losses correspond well in Fig 6 (a). Slightly lower losses can be observed in the simulations at no-load condition and with the 25 % load, but with higher loads the simulated losses match well with the measured ones. Very similar behaviour is observed at PWM supply in Fig. 6 b).
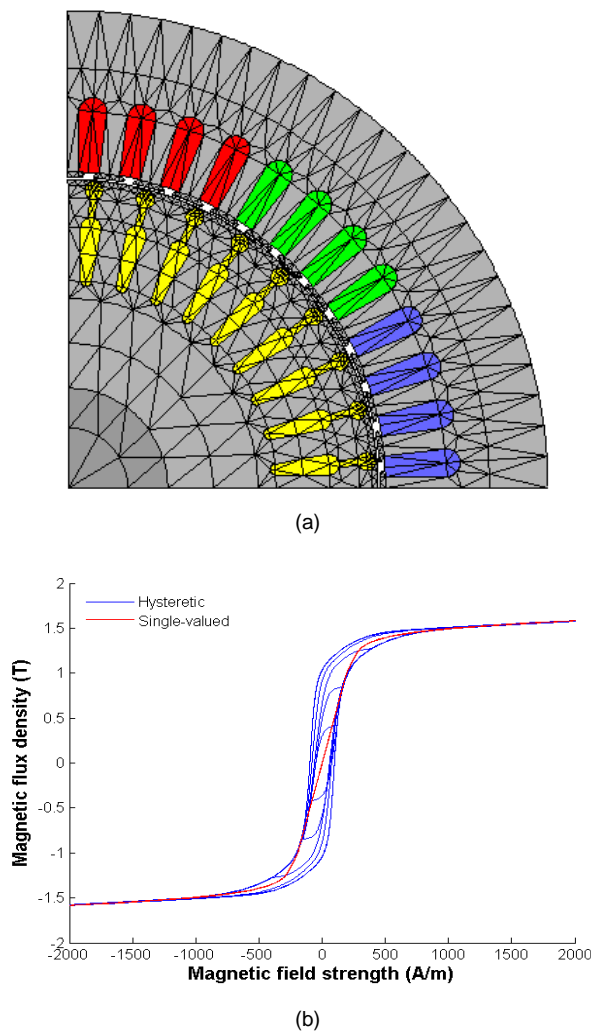
(a)

(b)

Fig. 5. (a) The 2nd-order FE mesh and (b) magnetization curves used in the simulations.

As seen in Fig. 6 c), at DPWM supply, the simulated and measured total losses are less coherent than with the DTC or PWM supply. Also, in this case the simulated losses are greater than the measured ones in the no-load and low load points. It should be pointed out that the same measurement protocol with the same measurement instruments and settings were used in all measurement points and from the measurement accuracy point of view, the DPWM supply is the most demanding one.

In the following sections the different components of the motor losses are analyzed. The measured losses are segregated by using the equations presented in Section II and they are compared with the components obtained with FEM analysis. The results of the analytical equations based on measured results are labeled in the Figs. 6 to 9 with "Anal." and the results obtained with finite element analysis with "FEM".

B. Stator Losses

The stator copper losses are related to the resistance value of the stator winding and RMS current flowing in the windings and they should remain almost similar with all
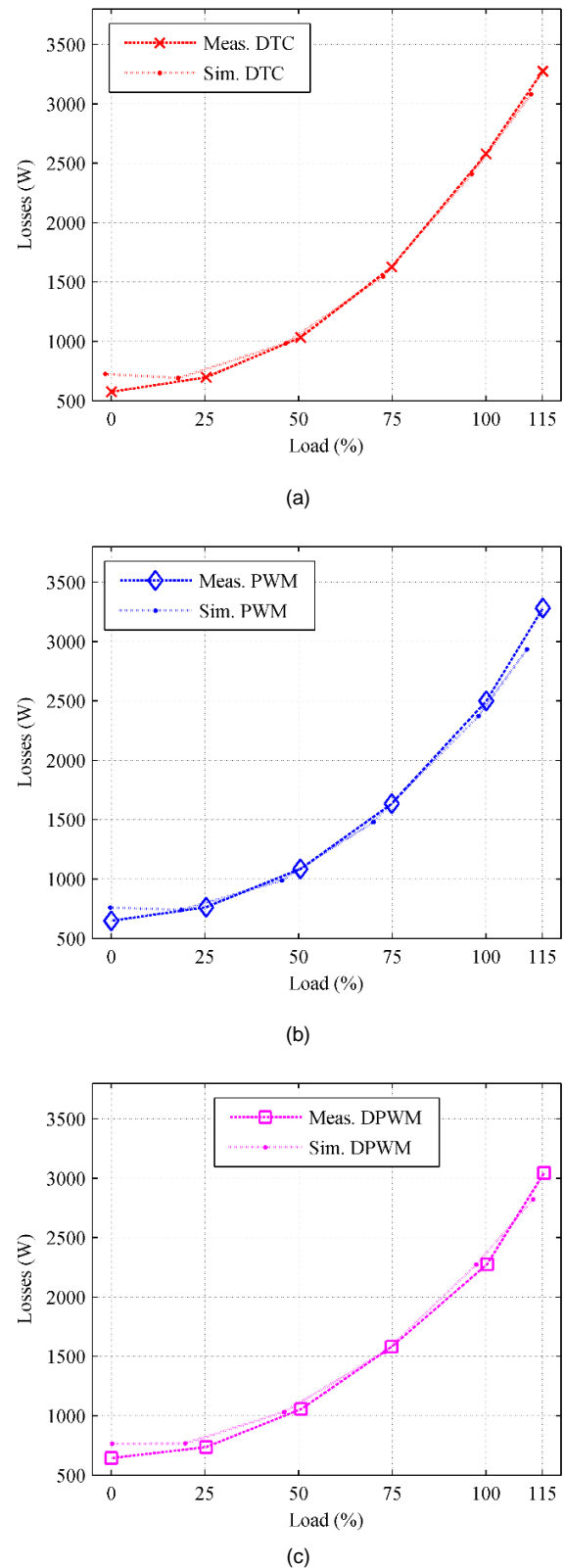

(a)

(b)

(c)

Fig. 6. Comparison of the measured and simulated total electromagnetic losses with (a) DTC, (b) PWM and (c) DPWM supplies. The measured total electromagnetic losses is obtained by subtracting the mechanical output power and the friction and windage losses of 152 W from the electric input power.

voltage supplies. The determined stator copper losses are given in Fig 7. The torque producing fundamental voltage amplitude applied to the motor terminals is smaller in the converter supply than with the sinusoidal supply, and thus the stator current and the stator copper losses are higher. The measured stator copper losses are calculated by using the corrected DC-resistance value according to the measured winding temperature and measured current. To get a more realistic approximation for the Joule losses, the AC-resistance should be used. The AC resistance can be calculated using different methods [35] and would allow accounting for the variation of the resistance due to the proximity and skin effects in the copper losses [36]. However, a winding manufactured with thin round enameled wires does not have significant extra AC-losses at these frequencies.

C. Iron Losses

We can assume that the magnitude of the conventional iron losses (traditional iron losses that are related to the fundamental wave magnetic flux) is similar with sinusoidal supply and with PWM-supply. The term conventional iron loss is very well explained in [37]. The measured and simulated iron losses are shown in Fig. 8. The measured iron losses are defined based on measured fundamental wave voltage at each load point. The increased measured iron losses due to PWM-supply will be considered in the residual losses part. The total iron losses calculated with the FE model increase with the loading, which supports the conclusions drawn in [38]. When the iron losses are determined in the inner voltage point according to IEC with a sinusoidal supply equal the motor rated voltage, the iron losses would be 425 W (labelled "IEC" in Fig. 8). The measured fundamental wave iron losses are decreasing as the fundamental wave voltage is decreasing due to increased resistive voltage drops in the converter with higher loads. The simulated iron losses behave very similarly with all the voltage supplies, even though the voltage spectrum is very different for DTC and carrier based modulation (Fig. 2.). The simulated iron losses are much higher than the analytically calculated based on measurements as expected, since the losses simulated with FEM include also the iron losses created by harmonics due to PWM. In the nominal load point the simulated iron loss is around 640 W which is 50 % higher than with sinusoidal supply according to IEC. The high increase in losses with converter supply can be a result of the high leakage reactance that are a result of the motor high-efficiency design.

D. Rotor Joule losses

The rotor winding Joule losses are formed by the currents in the aluminum rotor cage. The magnitude of the inductive current in the rotor depends on the rotor slip. The time harmonics in the air gap flux produce additional current components that create additional losses with distorted voltage waveforms. The measured and simulated rotor Joule losses are compared in Fig. 9. The measured rotor copper losses are overall smaller than the simulated ones. The measured rotor losses calculated based on analytical equations covers the extra losses that are due to the increased slip caused by extra
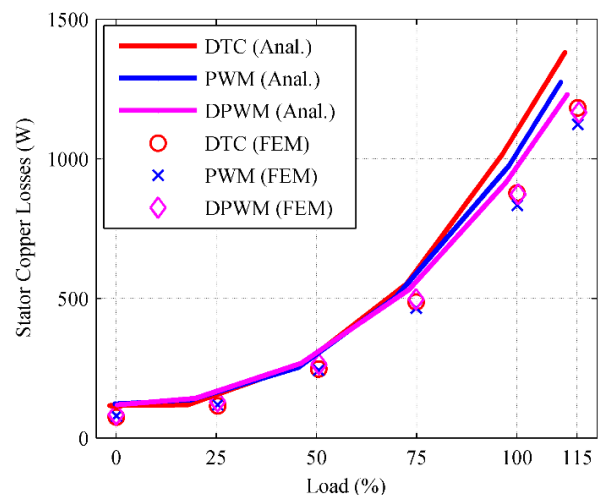

Fig. 7. Stator copper losses calculated analytically based on the measurement results and simulated with FEM.
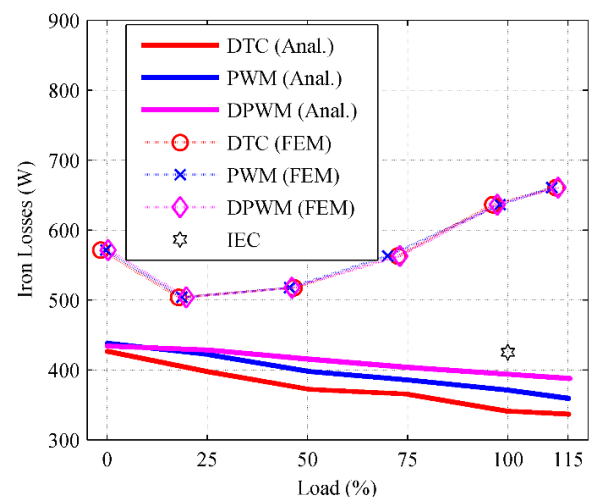

Fig. 8. Iron losses. The analytically calculated values include only the fundamental wave iron losses. The simulated values with FEM include the hysteresis, eddy current and excess losses. The difference between analytically calculated losses and the losses obtained with FEM can be considered as additional harmonic losses in the iron core caused by PWM- supply. The IEC labelled point shows the standard sinusoidal supply iron losses determined according to IEC 600034-2-1.

losses and temperature rise in the rotor due to PWM but it does not include the harmonic losses that based on increased harmonic loss components in the air-gap flux. Small amount of rotor Joule losses are observed in results obtained with FEM even in the no-load condition. The analytical equations are based on the assumption that the rotor current is negligible but FEM calculation is based on more realistic condition where small loss producing current is flowing in the rotor bars.

E. Additional load losses

The additional losses are the part of the motor losses that are not included in other loss components. In finite element analysis there is no loss component that can be considered as "non-modelled" losses, since all losses are based on loss models that describe a certain phenomenon. The difference between the sum of all simulated loss components and
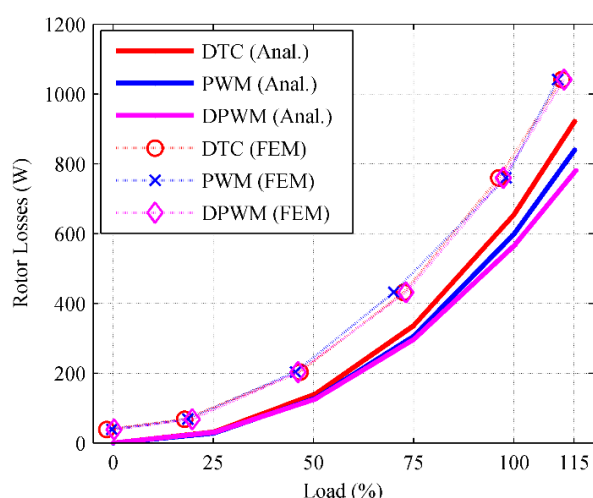
Fig. 9. Rotor Joule losses calculated analytically based on the measurement results and simulated with FEM.
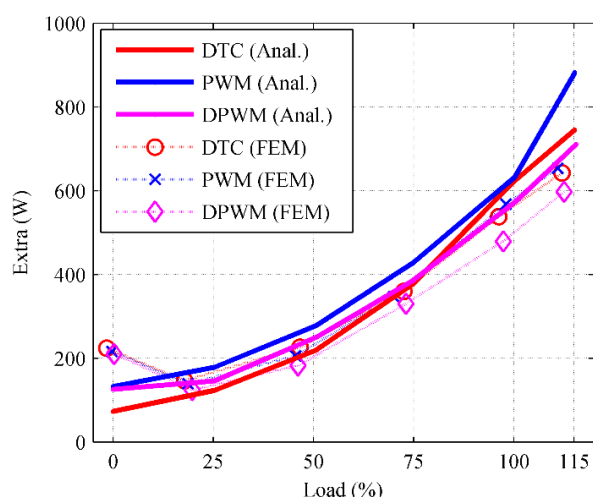

Fig. 10. The analytically calculated losses here are the sum of the additional load losses and the harmonic losses. The simulated loss components is the difference between the total measured electromagnetic losses and all simulated loss components because there cannot exist non-modelled losses in the simulation.

measured total losses and analytically calculated residual losses using measured values are presented in Fig. 10.

VII. CONCLUSIONS

The results here are based on only a single four-pole, 400 V, 37 kW motor and further studies have to be performed to obtain a commonly accepted way to determine and characterize the additional harmonic losses created by a PWM-supply. The conventional loss components can be used to roughly estimate where the losses of the induction motor take place. The additional load loss component can be considered to include all the losses that are not included in the other conventional loss components and also the PWM-created losses should be included in this part. When comparing the different modulation methods the switching frequency should be carefully analysed not to draw inconsistent conclusions based on wrong assumptions. The 50 Hz point is a rather complicated operating point for converter

fed induction motor analysis and several factors are affecting the overall losses. Here, fixed converter input voltage was used and due to minor technical differences between the three converters that were used, the fundamental wave voltages of the different modulation methods are not same and the results here cannot be directly use to rank the modulation methods. Based on the results in this paper, in type testing of the motors different modulation methods could be accepted since the loss tolerance of the IEC-efficiency classification is 15% (10% for larger machines) and generally speaking the effect of the modulation method on the motor losses is marginal. When considering the measurement accuracy of the different measurement systems that are used in the industry we cannot even expect that the few percent loss increase can be absolutely detected from the measurement results. The FE model gives convincing results and it can be rather easily used to extrapolate, interpolate and to segregate the motor losses in components.

REFERENCES

[1] A. Boglietti, A.M., EL-Refaie, O., Drubel, A.M., Omekanda, N. Bianchi, E.B. Agamloh, M. Popescu, A. Di Gerlando, J.B. Bartolo, "Electrical Machine Topologies: Hottest Topics in the Electrical Machine Research Community," *IEEE Industrial Electronics Magazine*, vol. 8, no. 2, pp.18-30, June 2014.

[2] A. Kosonen, L. Aarniovuori, J. Ahola, J. Backman, J. Pyrhönen, and M. Niemelä, "Loss definition of electric drives by a calorimetric system with data processing," *IEEE Trans. Ind. Electron.*, vol. 61, no. 8, pp. 4432–4442, August 2014.

[3] W. Cao, G.M. Asher, X. Huang, H. Zhang, I. French, J. Zhang, and M. Short, "Calorimeters and techniques used for power loss measurements in electrical machines," *IEEE Instrum. Meas. Mag.*, vol. 13, no. 6, pp. 26–33, December 2010.

[4] *Rotating electrical machines – Part 2-1. "Standard methods for determining losses and efficiency from tests (excluding machines for traction vehicles)*, Ed. 2, IEC 60034-2-1, June 2014..

[5] *Rotating Electrical Machines—Part 2–3: Specific Test Methods for Determining Losses and Efficiency of Converter-Fed AC Induction Motors*, IEC 60034-2-3 TS, 2013.

[6] L. Aarniovuori, L., Laurila, M. Niemelä, J. Pyrhönen, "Measurements and Simulations of DTC Voltage Source Converter and Induction Motor Losses," *IEEE Trans. Ind. Electron*, vol. 59, no. 5, pp. 2277-2287, May 2012.

[7] *Ecodesign for power drive systems, motor starters, power electronics and their driven applications – Part 2: Energy efficiency indicators for power drive systems and motor starters,* EN-50598, CENELEC(2014)

[8] I.P. Tsoumas, H. Tischmacher, P., Kollensperger, "The European Standard EN 50598-2: Efficiency classes of converters and drive systems," *in proc. International Conference on Electrical Machines (ICEM)*, Berlin, Germany, Sept. 2014. pp. 929–935.

[9] A. Boglietti, A., A. Cavagnino, M. Cossale, A. Tenconi, S. Vaschetto, "Efficiency determination of converter-fed induction motors: Waiting for the IEC 60034–2–3 standard," *in Proc. Energy Conversion Congress and Exposition (ECCE'13)*, Denver, CO, USA, Sep. 2013. pp. 230–237.

[10] J. Pippuri, A., Arkkio, "Challenges in the segregation of losses in cage induction machines," *in Proc. 18th International Conference on Electrical Machines (ICEM 2008),* Vilamoura, Portugal, Sep. 2008. pp.1–5.

[11] K., Dabala, "Analysis of mechanical losses in three-phase squirrel-cage induction motors," *in Proc. Fifth International Conference on Electrical Machines and Systems (ICEMS 2001)*, Shenyang, China, Aug. 2001, pp. 39–42.

[12] A. Boglietti, A. Cavagnino, M. Lazzari, M. Pastorelli, "International standards for the Induction Motor Efficiency Evaluation: Critical Analysis of the Stray-Load Loss Determination", *IEEE Trans. Ind. Applicat.*, Vol. 40, No. 5, Sept. 2004, pp. 1294–1301.

[13] M. Aoulkadi, "*Experimental Determination of Stray Load Losses in Cage Induction Machines*", Ph.D. Thesis, Darmstadt University of Technology, Germany, 2011.

[14] J.W. Kolar, H. Ertl, F. C. Zach, "Influence of the modulation method on the conduction and switching losses of a PWM converter system," *IEEE Trans. Ind. Applicat.*, vol. 27, no. 6, pp. 1063-1075, Nov. 1991.

[15] G.D. Holmes, T.A. Lipo, —Pulse Width Modulation for Power Converters - Principles and Practice, IEEE Press Series on Power Engineering, John Wiley and Sons, Piscataway, NJ, USA, 2003.

[16] F.J. Harris, "On the Use of Windows for Harmonics Analysis with the Discrete Fourier Transform," Proceedings of the IEEE, Vol. 66, No. 1, January 1978.

[17] M.J. Melfi, "Quantifying the Energy Efficiency of Motors on Inverters," *IEEE Industry Applications Magazine,* vol. 17, no. 6, pp.37–43, Dec. 2011.

[18] I. Takahashi ,T. Noguchi, "A new quick response and high efficiency control strategy of an induction motor," *IEEE Trans. Ind. Appl.*, vol. 22, no. 5, pp. 820–027, Sep. 1986.

[19] M. Depenbrock, "Direct self-control (DSC) of inverter-fed induction machine," *IEEE Trans. Power Electron.*, vol. 3, no. 4, pp. 420–429, Oct. 1998.

[20] J.-K. Kang and S.K. Sul, "Analysis and prediction of inverter switching frequency in direct torque control of induction machine based on hysteresis bands and machine parameters," *IEEE Trans. Ind. Electron.*, vol. 48, no. 3, pp. 545-553, June 2001.

[21] V. Ambrozic, M. Bertoluzzo, G.S. Buja, and R. Menis "An assessment of the inverter switching characteristics in DTC induction motor drives," *IEEE Trans. Power Electron.*, vol. 20, no. 2, pp. 457–465, March 2005.

[22] N.R.N. Idris, C.L. Toh, and M.E. Elbuluk, "A new torque and flux controller for direct torque control of induction machines," *IEEE Trans. Ind. Appl.*, vol. 42, no. 6, pp.1358–1366, Nov. 2006.

[23] N.R.N. Idris and A.H.M. Yatim, "Direct torque control of induction machines with constant switching frequency and reduced torque ripple," *IEEE Trans. Ind. Electron.*, vol. 51, no. 4, pp. 758–767, Aug. 2004.

[24] M. Hajian, J. Soltani, G.A. Markadeh, and S. Hosseinnia, "Adaptive nonlinear direct torque control of sensorless IM drives with efficiency optimization," *IEEE Trans. Ind. Electron.*, vol. 57, no. 3, pp.975–985, March 2010.

[25] C. Lascu, I. Boldea, and F. Blaabjerg, "Direct torque control of sensorless induction motor drives: a sliding-mode approach," *IEEE Trans. Ind. Appl.*, vol. 40, no. 2, pp. 582–590, March 2004.

[26] K.-K. Shyu, J.K. Lin, V.-T. Pham, M.-J. Yang, and T.-W. Wang, "Global minimum torque ripple design for direct torque control of induction motor drives," *IEEE Trans. Ind. Electron.*, vol. 57, no. 9, pp. 3148–3156, Sept. 2010.

[27] J.-K. Kang and S.-K. Sul, "New direct torque control of induction motor for minimum torque ripple and constant switching frequency", *IEEE Trans. Ind. Appl.*, vol. 35, no. 5, pp.1076–1082, Sep. 1999.

[28] P. Pohjalainen, P. Tiitinen, and J. Lalu, "The next-generation motor control method-direct torque control, DTC." *In Conf. Rec. EPE'94*, Orlando, FL, U.S.A., 1994. pp. 115–120.

[29] Z. Keliang, W. Danwei, "Relationship between space-vector modulation and three-phase carrier-based PWM: a comprehensive analysis [three-phase inverters]," *IEEE Trans. Ind. Electron.*, vol. 49, no. 1, pp.186–196, Feb. 2002.

[30] D. G. Holmes, "The significance of zero space vector placement for carrier-based PWM schemes," *IEEE Trans. Ind. Applicat.*, vol. 32. No. 5, pp. 1122–1129, Sept. 1996.

[31] IEEE Recommended Practice and Requirements for Harmonic Control in Electric Power Systems," in *IEEE Std 519-2014 (Revision of IEEE Std 519-1992)*, pp.1–29, June 2014.

[32] A. Arkkio, "Analysis of Induction Motors Based on the Numerical Solution of the Magnetic Field and Circuit Equations," Doctoral Dissertation, Acta Polytechnica Scandinavica, Electrical Engineering Series, No. 59, 1987, 97 p. Available: http://lib.hut.fi/Diss/198X/isbn951226076X/.

[33] J. Lähteenmäki, "Design and Voltage Supply of High-Speed Induction Machines," Doctoral Dissertation, Acta Polytechnica Scandinavica, Electrical engineering Series, No. 108, 2002, 140 p. Available: http://lib.tkk.fi/Diss/2002/isbn951226224X/.

[34] P. Rasilo, E. Dlala, K. Fonteyn, J. Pippuri, A. Belahcen, and A. Arkkio, "Model of Laminated Ferromagnetic Cores for Loss Prediction in Electrical Machines," *IET Electr. Power Appl.*, Vol. 5, No. 5, pp. 580-588, August 2011.

[35] A. Reatti, M.K., Kazimierczuk, "Comparison of various methods for calculating the AC resistance of inductors," *IEEE Transactions on Magnetics*, vol. 38, no. 3, pp.1512–1518, May 2002.

[36] D.A., Gonzalez, D.M., Saban, "Study of the Copper Losses in a High-Speed Permanent-Magnet Machine With Form-Wound Windings," *IEEE Tran. Ind. Electron.*, vol. 61, no. 6, pp. 3038–3045, June 2014.

[37] Z. Gmyrek, Z, A. Boglietti, A. Cavagnino, "Estimation of Iron Losses in Induction Motors: Calculation Method, Results, and Analysis," *IEEE Trans. Ind. Electron*, vol. 57, no. 1, pp.161–171, Jan. 2010.

[38] L.T. Mthombeni, P. Pillay, "Core losses in motor laminations exposed to high-frequency or nonsinusoidal excitation," *IEEE Trans. Ind. Applicat*, vol. 40, no. 5, pp.1325–1332, Sept. 2004.

Lassi Aarniovuori (M'15) was born in Jyväskylä, Finland, in 1979. He received the M.Sc. and D.Sc. degrees in electrical engineering from Lappeenranta University of Technology (LUT), Lappeenranta, Finland, in 2005 and 2010, respectively.

He is currently a Post-doctoral Researcher in the Department of Electrical Engineering, LUT. His current research interests include the field of electric drives, especially simulation of electric drives, efficiency measurements, and calorimetric measurement systems.

Paavo Rasilo received his M.Sc. (Tech.) and D.Sc. (Tech.) degrees from Helsinki University of Technology (currently Aalto University) and Aalto University, Espoo, Finland in 2008 and 2012, respectively. He is currently working as an Assistant Professor at the Department of Electrical Engineering, Tampere University of Technology, Tampere, Finland. His research interests deal with numerical modeling of electrical machines as well as power losses and magnetomechanical effects in soft magnetic materials.

Markku Niemelä was born in Mäntyharju, Finland, in 1968. He received the B.Sc. degree in electrical engineering from Helsinki Institute of Technology in 1990, and the M.Sc. and D.Sc. (technology) degrees from Lappeenranta University of Technology (LUT), Lappeenranta, Finland, in 1995 and 1999, respectively.

He is currently a Senior Researcher with the Carelian Drives and Motor Centre in LUT. His current research interests include motion control, control of line converters, and energy efficiency of electric drives.

Juha J. Pyrhönen (M'06) born in 1957 in Kuusankoski, Finland, received the Doctor of Science (D.Sc.) degree in electrical engineering from Lappeenranta University of Technology (LUT), Finland in 1991. He became Professor of Electrical Machines and Drives in 1997 at LUT. He is engaged in research and development of electric motors and power-electronic-controlled drives. Prof. Pyrhönen has wide experience in the research and development of special electric drives for distributed power production, traction drives and high-speed applications. Permanent magnet materials and applying them in machines have an important role in his research. Currently he is also researching new carbon-based materials for electrical machines